Journal of Non-Newtonian Fluid Mechanics 320 (2023) 105102

Contents lists available at ScienceDirect

Journal of Non-Newtonian Fluid Mechanics

journal homepage: www.elsevier.com/locate/jnnfm

Multiple inlet sudden expansion flow of power-law fluids

C.G. Carson [a], J.L. Cummings [a], R.J. Poole [b], K. Zografos [a,c], M.S.N. Oliveira [a,*]

[a] James Weir Fluids Laboratory, Department of Mechanical and Aerospace Engineering, University of Strathclyde, 75 Montrose Street, Glasgow, G1 1XJ, UK
[b] School of Engineering, University of Liverpool, Brownlow Hill, Liverpool, L69 3GH, UK
[c] Altair, 1 Rutland Court, Off Rutland Square, Edinburgh EH3 8FL

ARTICLE INFO

Dataset link: https://doi.org/10.15129/469a40a7-77ff-42b7-86ae-75797e09b934

Keywords:
Sudden expansion
Multiple inlets
Power-law fluids
Flow bifurcation

ABSTRACT

The flow of power-law fluids through two-dimensional planar sudden expansion geometries with multiple inlets was simulated numerically using an in-house finite volume code. The fluids are modelled using the power-law model, and a range of power-law index values ($0.4 \leq n \leq 1.4$) was investigated to cover shear-thinning, Newtonian and shear-thickening inelastic behaviour. The effect of the generalised Reynolds number and the spacing between inlets on the flow behaviour and stability was analysed. The main characteristics of the vortices formed near the wall are similar to those found in single inlet sudden expansions, with symmetric wall vortices forming at low Reynolds numbers, with transitions to steady asymmetric, third eddy flow regimes and time-dependent flow at higher generalised Reynolds numbers. In some cases, the steady asymmetric and third eddy regimes are absent and the flow transitions directly from symmetric flow to time dependent flow (as seen for the geometry with the largest spacing). The stabilising nature of shear-thinning behaviour was observed while the opposite effect was seen for shear-thickening behaviour. In addition, intermediate vortices were seen to form between inlets which grow in size within the symmetric regime as the generalised Reynolds number is increased. New scalings which help collapse the data are introduced and a strong effect of inlet spacing on all flow transitions is shown, with the ratio of the wall distance to inlet height being a determining factor on the corner vortices length when the spacing between inlets is sufficiently large.

1. Introduction

The flow of fluids through expansions is often encountered in nature (e.g. porous media flows and physiological flows), and in a wide range of engineering applications from pharmaceutical, to manufacturing and food production. The study of the fluid flow through simplified model geometries has over the years enhanced our understanding of the underlying physics and appreciation of the behaviours observed in real applications (for example as discussed in Browne et al. [1] in the context of flow through porous media).

Sudden expansion flows with a single inlet and a single outlet are often considered in the literature, including axisymmetric [2–4], square-square [5,6], planar [7,8], and truly two-dimensional (2D) [9–12] configurations. Early studies on flow bifurcation in sudden expansions focused on flows of Newtonian fluids. The seminal experimental work of Durst et al. [7] in 1974 utilised laser-Doppler anemometry (LDA) to study the flow through a planar 1:3 expansion and reported that the resulting flow is highly dependent on the Reynolds number, with two symmetric eddies forming along the walls downstream of the expansion for low Reynolds number. Upon increasing the Reynolds number, the flow is seen to undergo a supercritical pitchfork bifurcation in which the flow becomes asymmetric but remains steady. A further increase in Reynolds results in a third eddy forming downstream of the smaller of the two asymmetric eddies. Studies by Cherdron et al. [13] and Fearn et al. [8] expanded upon the work of Durst et al. [7] on 1:3 planar sudden expansions and confirmed the same general behaviour. Cherdron et al. [13] also discussed the effect of the aspect ratio (i.e. the normalised width of the channel) of the channel on the onset of these transitions, which introduced a further degree of complexity. To avoid the complexity introduced by three-dimensional (3D) effects, numerical works often consider the limit of truly 2D flows. In 1997, the numerical work of Alleborn et al. [14] reported values of critical Reynolds number in good agreement with the previous work of Cherdron et al. [13]. In addition, they examined the effect of the expansion ratio (ER), defined as the ratio of the outlet height to the inlet height, and found it had a strong influence on the critical Reynolds number. In the limit of expansion ratio approaching infinity, the critical Reynolds decreases asymptotically to a finite value; when the expansion ratio decreases, approaching unity (straight channel), it causes the critical Reynolds to increase rapidly. Although the

* Corresponding author.
E-mail address: monica.oliveira@strath.ac.uk (M.S.N. Oliveira).

https://doi.org/10.1016/j.jnnfm.2023.105102
Received 6 July 2022; Received in revised form 18 July 2023; Accepted 21 July 2023
Available online 26 July 2023

previous study only reported the values of critical Reynolds for a small number of expansion ratios, the trend of decreasing critical Reynolds numbers as the expansion ratio is increased was again reported by Drikakis [9] for a larger range of expansion ratios.

The previously discussed papers all consider Newtonian fluids, although it is common for the fluids used in relevant applications to show more complex rheological behaviour [15]. When investigating such fluids, it is helpful to start with simple rheological behaviour, e.g. inelastic fluids exhibiting shear-thinning or shear-thickening behaviour. The Ostwald De Waele model, commonly referred to as the power-law model, is a popular choice to model inelastic shear-dependent behaviour due to its simplicity as it requires only two parameters, the power-law index, n, and the consistency index, k [16]. When dealing with power-law fluids it is customary to define a generalised Reynolds number, such that in fully developed flow the product of the generalised Reynolds number ($\mathrm{Re}_{\mathrm{gen}}$) and the friction factor remains constant and equal to its Newtonian value [17]. The expression of $\mathrm{Re}_{\mathrm{gen}}$ for 2D flows adopted in the present work is reported in Section 2.2, with the terminology Reynolds number and the generalised Reynolds number used interchangeably henceforth.

In a study performed by Manica and De Bortoli [18] considering a 1:3 planar sudden expansion, the authors employed the power-law model and varied the power-law index within the range 0.2 to 2 for different Reynolds numbers. They found that shear-thinning behaviour acted to increase the critical Reynolds, whereas for shear-thickening fluids they reported the opposite behaviour. Although, it was later shown that the wrong inlet boundary conditions were used in the study of Manica and De Bortoli [18], Neofytou [11] showed the same qualitative trend when investigating a 1:2 planar sudden expansion, using both the power-law model and the Casson model, in which the power-law index was varied from 0.3 to 3. Pinho et al. [4] also reported this trend in an axisymmetric sudden expansion of diameter ratio 1:2.6. Further, Ternik et al. [10] employed a quadratic model to simulate the behaviour of a corn-starch and water mixture and then compared the results with those obtained from the power-law model. They again found that, relative to Newtonian fluid flows, shear-thickening behaviour results in a decrease of the critical Reynolds number for the flow bifurcation from symmetric to asymmetric flow. Furthermore, they showed that it also acts to increase the reattachment length, effectively meaning that for similar conditions of $\mathrm{Re}_{\mathrm{gen}}$, shear-thickening fluids exhibit eddies longer than Newtonian counterparts. Later, Ternik [19] performed similar research into shear-thinning fluids and found they displayed contrasting behaviour, in that the reattachment length of shear-thinning fluids was reduced when compared to the Newtonian. Again expanding the knowledge base, Ternik investigated both shear-thinning and shear-thickening fluids under creeping and low Reynolds number flow conditions ($0.0001 \leq \mathrm{Re}_{\mathrm{gen}} \leq 10$) [20]. The study showed that under creeping flow conditions, Moffatt eddies are formed in the salient corners downstream of the expansion which do not grow with $\mathrm{Re}_{\mathrm{gen}}$. Rather, the flow separation point is moved closer to the sharp re-entrant corner and the reattachment point is moved farther away from the expansion plane as n is increased. The growth of these vortices then tends to a linear relationship with $\mathrm{Re}_{\mathrm{gen}}$ as the flow conditions move away from creeping flow into the slowly moving regime. Dhinakaran et al. [12] provided benchmark quality data for power-law fluid flows in the now standard 1:3 expansion geometry using an in-house finite-volume code. Whilst reporting similar trends and behaviours to previous studies they investigated a larger range of power-law index (from 0.2 to 4), for both creeping and inertial flows (covering a range of $\mathrm{Re}_{\mathrm{gen}}$ from 0.01 to 600).

Flows within more complex geometries (such as contraction-expansions) and/or considering fluids with more complex rheological responses, such as viscoplasticity or viscoelasticity have also been considered. These responses increase complexity and are not examined in the present study which focuses on inelastic fluid flows and thus will not be discussed here. However the reader is referred to the studies investigating expansion [21–27] or contraction–expansion flows [28–35] and the references within for more information.

All studies mentioned previously investigated the effects of single inlet sudden expansions, however, in real applications the geometry of such expansions is not limited to this case and often displays complex configurations that can manipulate the number of inlets, their size and spacing, together with the flow rate or velocity through each inlet. In one such study, Ameur [36] examined the flow of shear-thinning fluids modelled using the power-law model in axisymmetric multi-inlet stream geometries and varied several geometric parameters, e.g. the number of inlets and spacing between inlets. The study showed that for a power-law index of $n = 0.75$ (corresponding to shear-thinning fluid behaviour) in a two-inlet geometry, reducing the spacing between inlets gives rise to more complex behaviour of the eddies in the corners of the sudden expansion, whereas an increased spacing suppresses these corner vortices. Further, multiple inlet geometries give rise to vortices formed between each inlet stream, which grow in size when the inlet spacing is increased.

In the present study, we investigate numerically the flow of inelastic fluids described by the power-law model through 2D multiple inlet sudden expansion geometries of variable inlet spacing. We consider the flow of not only Newtonian ($n = 1$) and shear-thinning ($n < 1$) fluids, but also shear-thickening fluids ($n > 1$), and provide a systematic study on the combined effects of the generalised Reynolds number, the spacing between inlets and the power-law index on the flow behaviour and bifurcations, critical Reynolds numbers, vortex lengths and intensities. The paper proceeds in the following manner: Section 2 presents the mathematical formulation and problem description; Section 3 details the numerical method employed; Section 4 presents and discusses the results, including the effect of power-law index and geometric parameters (e.g. inlet spacing and distance to the wall); Section 5 summarises the major findings of the study.

2. Problem description

2.1. Problem geometry

The geometry of the problem being studied is presented in Fig. 1(a), where important geometrical variables are identified. Three individual 2D channels of height h, separated by spacing S, culminate in a sudden expansion into a single channel of height H. The flow is from left to right (i.e. in the positive x-direction), and the geometry is symmetric relative to $y = 0$. The spacing S is varied across 5 different geometric cases, with the magnitude of the spacing relative to the inlet channel height h defined by the spacing ratio SR ($SR = S/h$). This parameter ranges from $SR = 0.1$ when the inlets are closest, to $SR = 2$ when the inlets are furthest apart, as detailed in Table 1 and Fig. 2. The geometry displayed in Fig. 1 corresponds to the intermediate case of $SR = 1$, which from now on is referred to as the base geometry. Varying the spacing between the inlets has an effect on the distance from the wall to the outermost inlet, W (salient corner to the re-entrant corner). The magnitude of the distance W relative to the inlet channel height h is referred to as wall ratio WR ($WR = W/h$) with the values for each geometry detailed in Table 1. The origin of the geometry's coordinate system is located at the midpoint of the expansion plane (as shown in Fig. 1(a)). The length of each inlet channel is $20h$ to allow the flow to become fully developed prior to the expansion. Similarly, the length of the outlet channel downstream of the expansion is 20H (i.e. $180h$) to ensure the outlet is sufficiently far from the region of interest where flow recirculations develop. Following previous work in contraction flows with multiple inlets [37], we consider here the case with three inlets in addition to the reference case with the single inlet. The expansion ratio is defined as $ER = H/h$ and was chosen to be $ER = 9$, unless stated otherwise. In the triple inlet case, $ER = 9$ corresponds to an equivalent expansion ratio of $ER^* = H/(3h) = 3$ taking into account

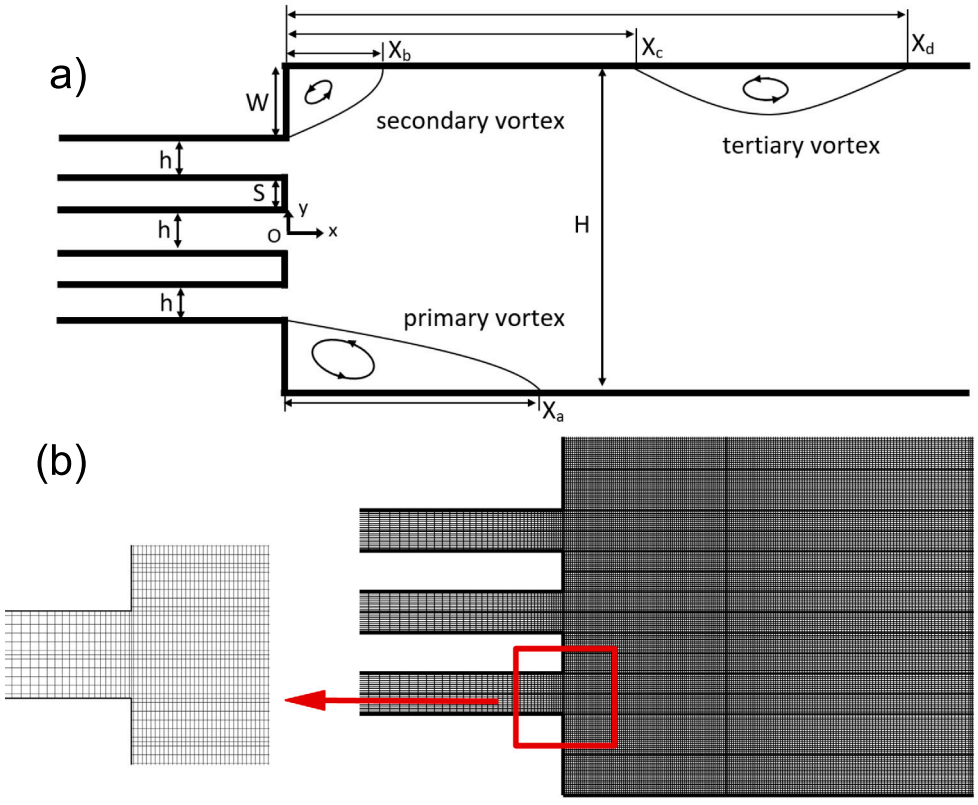

Fig. 1. (*a*) Schematics of the base geometry with three equal inlet channels and one larger outlet channel ($SR = 1$, $WR = 2$) and associated geometric parameters. (*b*) Mesh near the sudden expansion ($-5 \leq x/h \leq 10$), with zoomed view near the expansion for improved clarity. The flow is from left to right.

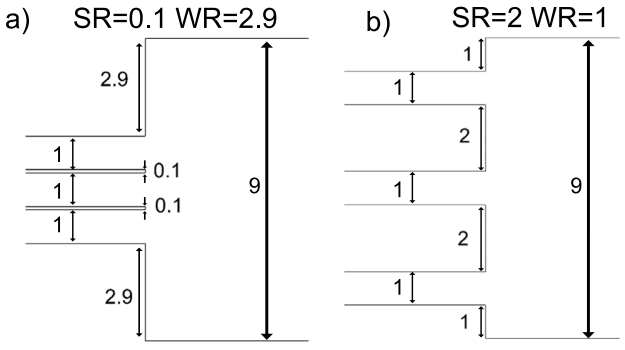

Fig. 2. Diagrams of geometry (*a*) A and (*b*) E showing the relevant normalised widths to highlight the differences as SR and WR are changed over the range of spacings.

the width of the three inlets. The value of this parameter was selected based on the design of the benchmark expansion geometry commonly employed in single inlet studies, which features a 1:3 expansion ratio [10,12,18–20]. The range of spacing ratios, SR, was varied between 0.1 and 2 to cover the complete range between the two limits of closely spaced inlets (Fig. 2(*a*)), akin to the single inlet 1:3 expansion case, to highly spaced inlets, with the outer inlets being located close to the lateral walls (Fig. 2(*b*)). It should be noted that when the number of inlets j (in this case $j = 3$) and the expansion ratio ER (in this case $ER = 9$) are fixed, changing SR controls WR, and in our case $SR + WR = 3$.

Table 1
Geometric parameters of each geometry investigated.

Geometry	ER	SR	WR
A	9	0.1	2.9
B	9	0.5	2.5
C (Base)	9	1	2
D	9	1.5	1.5
E	9	2	1

2.2. Governing equations

The flow under investigation is laminar and incompressible and is governed by the continuity equation,

$$\nabla \cdot \mathbf{u} = 0 \tag{1}$$

and the momentum equations:

$$\rho\left(\frac{\partial \mathbf{u}}{\partial t} + \mathbf{u} \cdot \nabla \mathbf{u}\right) = -\nabla p + \nabla \cdot \boldsymbol{\tau} \tag{2}$$

where $\mathbf{u}$ is the velocity vector, p is the pressure, ρ is the fluid's density and $\boldsymbol{\tau}$ is the extra stress tensor defined as:

$$\boldsymbol{\tau} = \eta(\dot{\gamma})\dot{\boldsymbol{\gamma}} \tag{3}$$

The fluids are modelled using the power-law model, with the viscosity function given by:

$$\eta(\dot{\gamma}) = K\dot{\gamma}^{n-1} \tag{4}$$

where n is the power-law index, K is the consistency index and $\dot{\gamma}$ is the magnitude of the shear rate tensor evaluated as:

$$\dot{\gamma} = \sqrt{\frac{\dot{\boldsymbol{\gamma}} : \dot{\boldsymbol{\gamma}}}{2}} = \sqrt{2\left(\frac{\partial u}{\partial x}\right)^2 + 2\left(\frac{\partial v}{\partial y}\right)^2 + \left(\frac{\partial u}{\partial y} + \frac{\partial v}{\partial x}\right)^2} \tag{5}$$

Table 2
Mesh characteristics of the geometries used in the mesh dependency study for $SR = 1$ and $WR = 2$.

Mesh	No. Cells	$\Delta x_{min}/h$	$\Delta y_{min}/h$	Max $\Delta L/L$ (%)
Mesh 1	22 080	0.1	0.1	8.3
Mesh 2	44 160	0.05	0.1	3.7
Mesh 3	88 320	0.05	0.05	–

The generalised Reynolds number ($\mathrm{Re}_{\mathrm{gen}}$) adopted in this work is defined based on conditions at the inlet, as in previous studies with power-law fluids [10,12]. It is defined such that, in fully developed channel flow, the product of $\mathrm{Re}_{\mathrm{gen}}$ and the friction factor remains constant and equal to its Newtonian value.

$$\mathrm{Re}_{\mathrm{gen}} = \frac{6\rho\bar{u}^{(2-n)}h^n}{K[(4n+2)/n]^n} \tag{6}$$

2.3. Boundary conditions

No-slip conditions are applied at the walls, while a uniform velocity field is imposed at the inlet. At the outlet, pressure is calculated through linear extrapolation of the two upstream cells, whereas vanishing gradients ($\frac{\partial u}{\partial x} = \frac{\partial v}{\partial x} = 0$) are assumed for velocity, as described in more detail in Oliveira et al. [38] and Dhinakaran et al. [12].

3. Numerical method

3.1. Solution

The in-house academic finite-volume code solves the governing equations utilising a method that is described in detail in Alves et al. [39], and Oliveira et al. [38], employing the SIMPLEC pressure correction algorithm for collocated cell arrangement, and so shall only be described briefly. The convective terms in the momentum equation are discretised using the CUBISTA high-resolution scheme [39], while the central difference scheme was used for the discretisation of diffusive terms and a first-order implicit Euler scheme for time derivatives [12,38]. The computational domain is partitioned into various blocks following the same approach as in Dhinakaran et al. [12]. The mesh is uniform in the transverse direction throughout all blocks. Mesh refinement in the streamwise direction is higher near the expansion plane where gradients are expected to be larger (see Fig. 1(*b*)). In the present study, the block immediately after the expansion exhibits a uniform mesh in the streamwise direction, with the meshes in all other blocks being either stretched or compressed in a geometric progression to provide a smooth transition from a coarser mesh at the inlet and outlet to a more refined mesh near the expansion (see Table 2).

3.2. Mesh dependency study

To investigate the dependency of the results on the mesh density, analysis of all vortex lengths along the wall (to $\mathrm{Re}_{\mathrm{gen}} = 50$ for the range $0.4 \leq n \leq 1.4$) was carried out using three different meshes of varying density for the geometry with intermediate spacing ratio, with the results presented in Table 2. As can be seen using Mesh 2 (intermediate mesh density) resulted in a maximum difference in vortex length relative to the most refined mesh of 3.7%, which was deemed acceptable. All further data presented in this paper have been generated with equivalent intermediate meshes unless stated otherwise.

4. Results and discussion

4.1. Base case flow

The first case we analyse considers the base geometry ($SR = 1$, $WR = 2$) and a Newtonian fluid ($n = 1$). To aid in visualisation of the flow and its different regimes, streamline plots are presented in Fig. 3. Similarly to the single inlet case, we observe different flow regimes as the $\mathrm{Re}_{\mathrm{gen}}$ is increased: symmetric flow, with the two corner vortices formed downstream of the expansion exhibiting the same length (Fig. 3(*a*)); asymmetric flow, with one vortex larger than the other (Fig. 3(*b*)) observed above a first critical Reynolds number ($\mathrm{Re}_{\mathrm{gen,cr1}}$); asymmetric flow with tertiary eddy formed downstream of the smaller vortex (Fig. 3(*c*)) above a second critical Reynolds number ($\mathrm{Re}_{\mathrm{gen,cr2}}$); and eventually time-dependent flow, where the size of the vortices varies in time (not shown). Here, the $\mathrm{Re}_{\mathrm{gen}}$ for each exemplifying streamline plot is taken relative to the critical values of $\mathrm{Re}_{\mathrm{gen}}$ following the approach of Dhinakaran et al. [12] for comparison between the various cases. The selected values of $\mathrm{Re}_{\mathrm{gen}}$ being slightly below $\mathrm{Re}_{\mathrm{gen,cr1}}$ (i.e. $\mathrm{Re}_{\mathrm{gen}} = 0.8\mathrm{Re}_{\mathrm{gen,cr1}}$) corresponding to symmetric flow; halfway between $\mathrm{Re}_{\mathrm{gen,cr1}}$ and $\mathrm{Re}_{\mathrm{gen,cr2}}$ (i.e. $\mathrm{Re}_{\mathrm{gen}} = 0.5(\mathrm{Re}_{\mathrm{gen,cr1}} + \mathrm{Re}_{\mathrm{gen,cr2}})$) corresponding to asymmetric flow, and slightly above $\mathrm{Re}_{\mathrm{gen,cr2}}$ (i.e. $\mathrm{Re}_{\mathrm{gen}} = 1.2\mathrm{Re}_{\mathrm{gen,cr2}}$) corresponding to asymmetric flow with a third eddy (or "3rd eddy" for short).

To quantify the effect of $\mathrm{Re}_{\mathrm{gen}}$ on the flow behaviour we analyse the normalised length ($L_R = X_R/h$) of the corner vortices formed downstream of the expansion (where subscript R refers to recirculation "a" or "b" corresponding to X_a and X_b identified in Fig. 1a) as well as their normalised intensity, Ψ_R. The intensity of the recirculation represents the total flow rate inside the recirculation in excess of the total inlet flow rate and is calculated by integration of the stream function $\psi = \frac{\partial u}{\partial y}$. The values of the normalised intensity of the corner recirculations shown here have been normalised using the flow rate through one of the inlets as reference: $\Psi_R = (\psi_R - 3\psi_h)/\psi_h = \psi_R/\psi_h - 3$, where ψ_R is the maximum value of ψ at the centre of the corner recirculation, and ψ_h is the value in each of the inlet channels (equal to the imposed flow rate in each inlet channel per unit depth). In addition, we also quantify the normalised lengths L_c and L_d associated with the tertiary vortex (corresponding to X_c and X_d identified in Fig. 1a).

The bifurcation plots as a function of $\mathrm{Re}_{\mathrm{gen}}$ for the base case geometry ($SR = 1$, $WR = 2$) and a Newtonian fluid, $n = 1$ (corresponding to Fig. 3) are shown in Fig. 4. Starting at low values of $\mathrm{Re}_{\mathrm{gen}}$, the flow is symmetric and the vortices formed in the two outer corners downstream of the expansion plane are equal in size ($L_a = L_b$) and intensity ($\Psi_a = \Psi_b$) and grow with increasing $\mathrm{Re}_{\mathrm{gen}}$. When the value of $\mathrm{Re}_{\mathrm{gen}}$ is increased above a certain point, termed as the first critical point $\mathrm{Re}_{\mathrm{gen,cr1}}$, there is a symmetry breaking bifurcation and one of the corner vortices becomes longer than the other, but the flow remains steady. The normalised length of the longer of the two vortices shall always be referred to as L_a and will be presented in streamline plots as being attached to the "lower" wall for consistency, however, the bifurcation is bi-stable and symmetry breaking in the opposite manner is equally as likely. In the vicinity of this $\mathrm{Re}_{\mathrm{gen,cr1}}$ the growth of both vortices is non-linear with L_a initially increasing and L_b initially decreasing. For larger $\mathrm{Re}_{\mathrm{gen}}$, the intensity and size of the larger vortex increase with $\mathrm{Re}_{\mathrm{gen}}$ is much more significant than that of the smaller vortex. A further increase in $\mathrm{Re}_{\mathrm{gen}}$ causes a second transition, termed $\mathrm{Re}_{\mathrm{gen,cr2}}$, where a third eddy forms on the wall downstream of the smaller of the two asymmetric vortices. Similar non-linear behaviour occurs before settling to near constant growth rates, with the growth rate of L_d being notably larger than the others. These three flow regimes, the symmetric, asymmetric, and asymmetric with tertiary eddy, alongside the characteristic behaviour of the growth of the vortices is similar to the flow observed in single inlet single outlet geometries [10–12,19,20]. The mechanism by which bifurcations occur

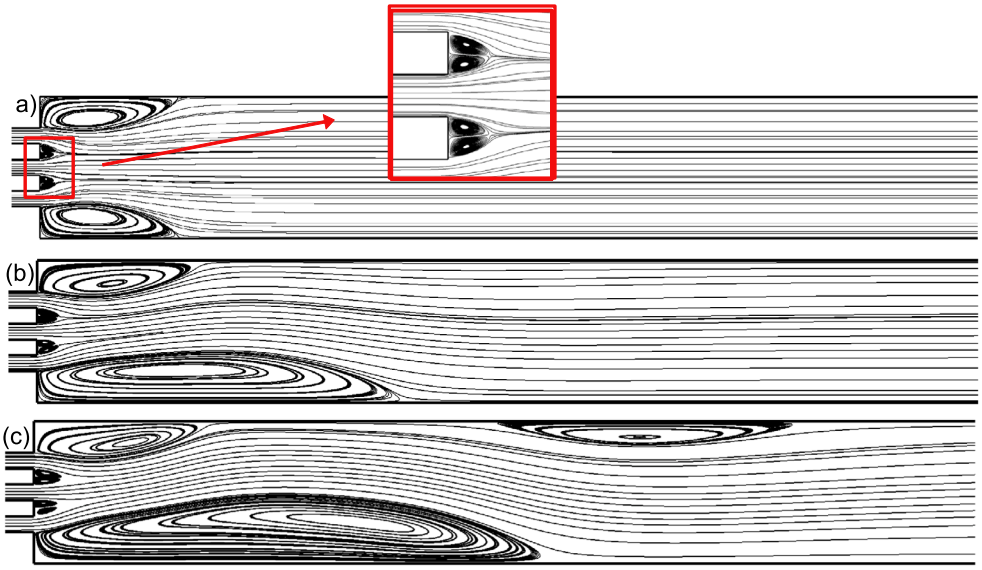

Fig. 3. Flow patterns in the (*a*) symmetric regime ($Re_{gen} = 0.8Re_{gen,cr1}$) with insert to highlight the intermediate vortices, (*b*) asymmetric regime ($Re_{gen} = 0.5(Re_{gen,cr1} + Re_{gen,cr2})$) and (*c*) 3rd eddy regime ($Re_{gen} = 1.2Re_{gen,cr2}$), for a Newtonian fluid ($n = 1$) in the base geometry ($SR = 1$, $WR = 2$).

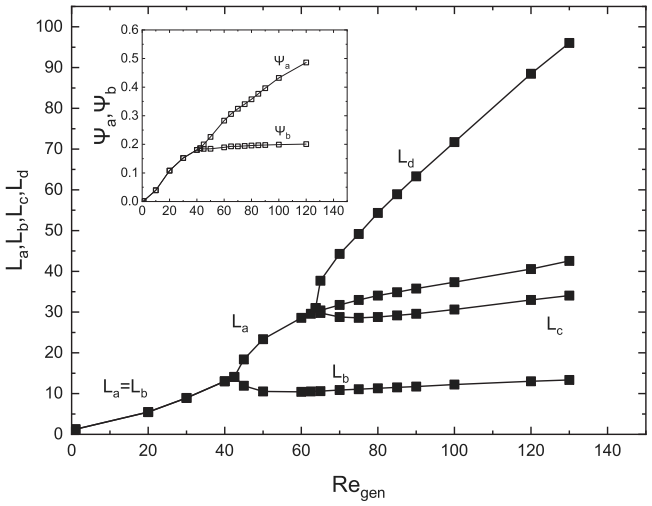

Fig. 4. Non-dimensional vortex length (L_R) variation against generalised Reynolds number for a Newtonian fluid ($n = 1$) in the base geometry ($SR = 1$, $WR = 2$). The inset shows the normalised corner vortex intensity (Ψ_R) as a function of Re_{gen} for the same case.

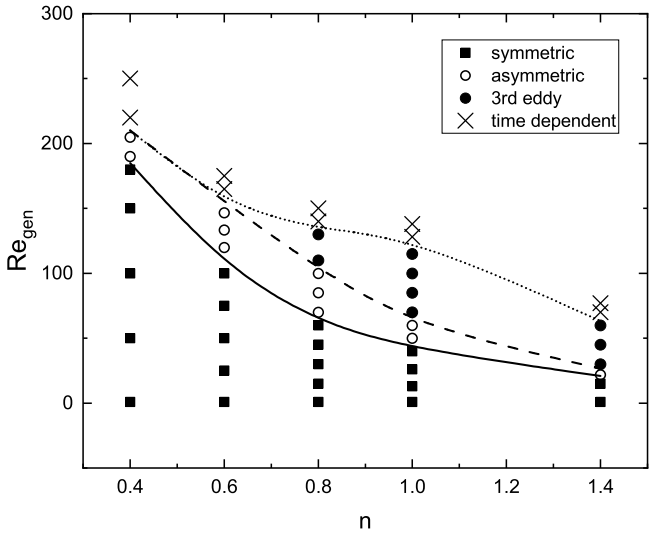

Fig. 5. $Re_{gen} - n$ flow map, showing the flow regimes and flow regime transitions present in the investigated range of Re_{gen} and power-law index for the base geometry ($SR = 1$, $WR = 2$). Lines are provided to guide the eye.

in planar sudden expansion flow has been associated with the Coanda effect [8,12,22]. Any perturbations to the flow at the expansion plane give rise to locally higher velocities and lower pressures, with respect to one side of the centreline, which then creates a transverse pressure gradient that acts to increase the deviation of the flow. At low Reynolds numbers, these perturbations may be damped by viscosity, whereas at the critical Reynolds number they are not and there is a supercritical transition to a new flow state that, although steady, is now asymmetric.

Fig. 3 also highlights the existence of two pairs of vortices formed at the expansion plane walls between inlet streams (as shown by the zoomed view in the inset of Fig. 3(*a*)). Within each individual pair the two vortices are always asymmetric, due to a lack of symmetry in the local flow conditions. However, it was observed that the two pairs are symmetric relative to the horizontal centreline ($y = 0$) and grow with increasing Re_{gen}, up until $Re_{gen,cr1}$. This confirms that up until $Re_{gen,cr1}$ the full flow, not just the corner vortices, is symmetric with respect to the geometric centreline ($y = 0$).

The Re_{gen} has been further increased to the point after which the flow becomes time dependent, with only steady values presented here. It is noted that the values of each critical point in the present study are quantitatively different from those in the aforementioned single inlet literature.

4.2. The effect of power-law index

In Fig. 5, we explore the Re_{gen} - n parameter space for the base geometry, displaying the transitions between the different flow regimes (symmetric, asymmetric, asymmetric with third eddy and time-dependent). The lines are indicative only to aid visualisation of the flow transitions. It can be seen that shear-thickening behaviour causes the flow to undergo the first bifurcation, from symmetric to asymmetric flow, at a lower $Re_{gen,cr1}$, with the opposite being observed for shear-thinning fluids. This is consistent with earlier studies in single inlet expansions [10–12,18]. The difference in the critical Reynolds numbers

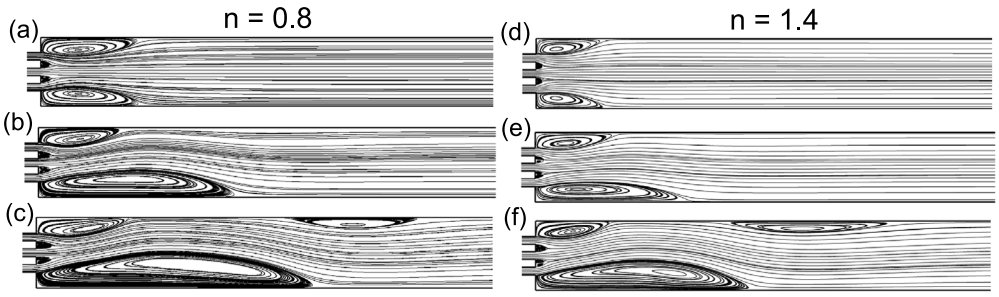

Fig. 6. Flow patterns in the (*a*, *d*) symmetric ($Re_{gen} = 0.8Re_{gen,cr1}$), (*b*, *e*) asymmetric ($Re_{gen} = 0.5(Re_{gen,cr1} + Re_{gen,cr2})$) and (*c*, *f*) 3rd eddy regime ($Re_{gen} = 1.2Re_{gen,cr2}$), for $n = 0.8$ (*a*–*c*), and $n = 1.4$ (*d*–*f*), for the base geometry ($SR = 1$, $WR = 2$).

between the different fluids arises from the competing effects of the shear-dependent viscosity and inertia on the size of the corner vortex [40,41]. In accordance with other results from the literature, the locations of flow separation and reattachment depend on the power-law index [10–12,18–20,40,41]. When the fluid is shear-thinning, the slower fluid in the corner vortex has higher viscosity compared to the faster fluid flowing outside of the vortex [40,41], and the outer fluid is not able to stretch the inner fluid resulting in the formation of smaller corner vortices for the same Re_{gen} compared to that of Newtonian and shear-thickening fluids. The opposite behaviour occurs for the shear-thickening fluids. Furthermore, for shear-thinning fluids, the near wall velocities are less sensitive to potential perturbations consummate with an increase of the value of the critical Reynolds number [12]. We also observe that the first region of asymmetric flow (when there is no third eddy) is reduced for shear-thickening fluids and becomes larger for shear-thinning fluids. For the cases of $n = 0.4$ and $n = 0.6$ the flow transitions directly from the steady asymmetric flow regime to the time dependent regime and no 3rd eddy regime observed. This shows that the transition to time dependent flow is not constrained to arise after the 3rd eddy regime. Again this mechanistic behaviour has been seen previously in the single inlet studies [12,18]. In terms of the transition to time-dependent flow, a decrease in n tends to stabilise the flow, delaying the transition to time-dependent flow to higher Re_{gen}.

Fig. 6 displays exemplifying streamline plots for a shear-thinning and shear-thickening case, created in the same way as Fig. 3 (i.e. at different Re_{gen} chosen to illustrate each flow regime: $0.8Re_{gen,cr1}$ (symmetric flow), $0.5(Re_{gen,cr1}+Re_{gen,cr2})$ (asymmetric flow), and $1.2Re_{gen,cr2}$ (asymmetric flow with tertiary eddy)). The first noticeable difference is in the size of the vortices, with the vortices in the shear-thinning case being larger. This increased length for the shear-thinning case is a manifestation of its increased stability allowing it to grow larger prior to bifurcation, which is in agreement with what was found in single inlet geometries [12].

Fig. 7 compares the effect of the Re_{gen} on both the normalised length of the recirculations (Fig. 7(*a*)) and the recirculation intensity (Fig. 7(*c*)) for the base geometry for an exemplifying shear-thinning fluid ($n = 0.8$), Newtonian fluid ($n = 1$) and shear-thickening fluid ($n = 1.4$). In the symmetric regime, the corner vortex size and intensity are seen to increase with Re_{gen} for all values of n studied. However, the stabilising effect of decreasing n is clearly visible, with the transitions being pushed to higher Re_{gen} for shear-thinning fluids. Further, it shows the difference in vortex growth rate which is particularly evident in the growth rate of L_d. It is interesting to note however that the size and intensity of the corner vortices at $Re_{gen,cr1}$ is similar for all n presented. Additionally, the size of the smaller asymmetric vortex L_b is also approximately the same for all n present. This can be seen more clearly in Fig. 7(*b*) where the curves for each value of power-law index are rescaled near the first critical point to show the normalised vortex sizes as a function of $\frac{Re_{gen}}{Re_{gen,cr1}} - 1$ where $Re_{gen,cr1}$ corresponds to the critical value for the relevant n. When scaled in this way the various data sets, both in terms of size (Fig. 7(*b*)) and intensity (Fig. 7(*d*)), corresponding to different n values nearly collapse, in particular in the symmetric flow regime. This similarity lessens for the higher Re_{gen} tested. In a similar way, the normalised size of the tertiary eddy ($L_d - L_c$) scales with $\frac{Re_{gen}}{Re_{gen,cr2}} - 1$ in the region of the second critical point, exhibiting a good overlap between the cases for different n as shown in the inset in Fig. 7(*b*).

4.3. The effect of geometry

4.3.1. The effect of SR

Fig. 8 presents streamline plots in the symmetric (Fig. 8(*a*)) and asymmetric (Fig. 8(*b*)) regimes across the range of SR studied for the case of a Newtonian fluid. As SR increases a decrease in the sizes of the corner vortices is seen, accompanied by a growth of the intermediate vortices. To show the quantitative effects of changing the spacing ratio SR, Fig. 9 presents similar plots to that of Fig. 5, for the various SR investigated. All plots exhibit the same scales to aid the comparison between the different cases considered, whilst the insets in Fig. 9(*c*) and (*d*) are zoomed to improve readability. The first point to note is the significant variation in the critical Re_{gen} for the transition to time dependent flow. As SR is decreased (i.e. inlets closer together) the flow remains steady until much higher values of Re_{gen}. For the case with the largest spacing ($SR = 2$; Fig. 9(*d*)), the decrease in the critical Re_{gen} for the transition to time dependent flow is particularly large and the flow does not exhibit any of the steady asymmetric regimes for the range of n studied. We believe this to be related to the differences in the redevelopment of the flow field downstream of the expansion plane and the presence/absence of the intermediate recirculations that form between the incoming streams, with the flow field in the closely-spaced inlet configurations (SR low, WR high) being less sensitive to perturbations compared to that in widely-spaced inlet configurations (SR high, WR low). For configurations with small SR, these intermediate vortices are attenuated or even nearly suppressed, as shown in the top image of Fig. 8(*a*) for $SR = 0.1$. While for larger SR (see e.g. the flow patterns depicted in the bottom image of Fig. 8(*a*) for $SR = 2$), these intermediate recirculations are "bound" between the higher velocity incoming streams, and more sensitive to potential perturbations in the flow field.

Another interesting effect is in the difference in $Re_{gen,cr1}$ as the spacing ratio changes. Considering the flow of a Newtonian fluid, the first critical Reynolds number varies from $Re_{gen,cr1} \approx 33$ when $SR = 0.1$, to $Re_{gen,cr1} \approx 42$ when $SR = 1$, to $Re_{gen,cr1} \approx 48$ when $SR = 1.5$ (as previously stated the geometry with the largest SR does not display a transition from steady symmetric flow to steady asymmetric flow). This behaviour is observed for all values of n studied and can be explained by introducing a modified expansion ratio, ER_{mod} ($ER_{mod} = \frac{H}{3h+2S} = \frac{ER}{3+2SR}$). Investigating the dependence between SR and ER_{mod}, it can be seen that as SR increases, ER_{mod} decreases, for the fixed ER employed in the current geometry. In single inlet geometries a decrease in the expansion ratio has been shown to have a stabilising effect on $Re_{gen,cr1}$ [9], with the same occurring here considering the

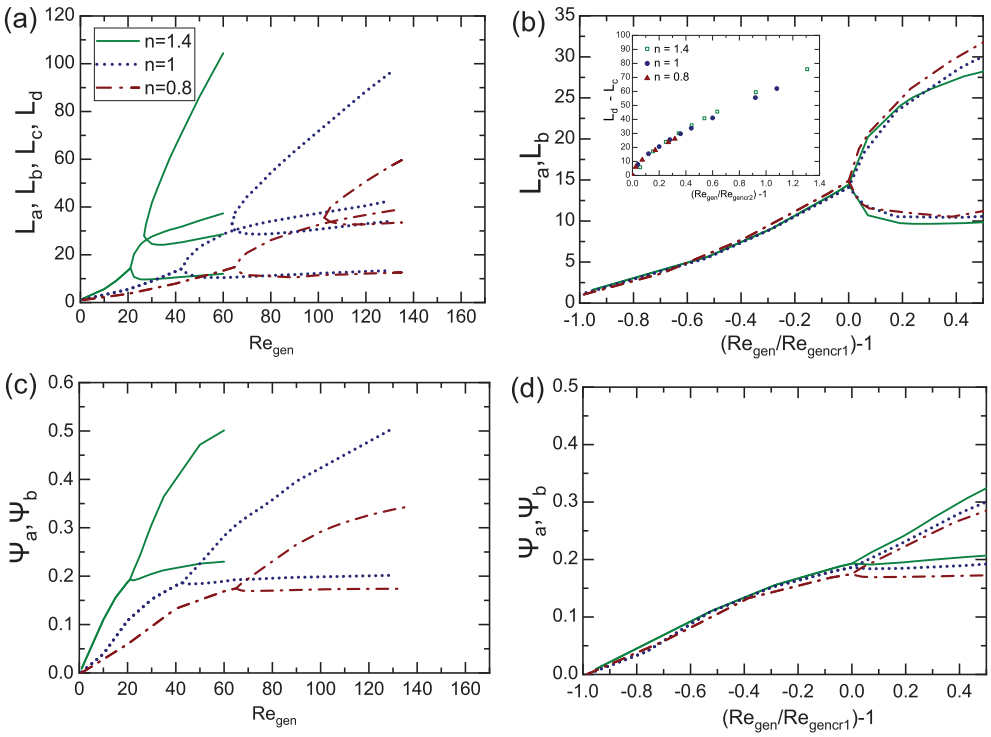

Fig. 7. Normalised vortex length (a, b) and intensity (c, d) against generalised Reynolds number for a range of fluids with different power-law index, in the base geometry (C: $SR = 1$ $WR = 2$). (a, c) presents the full range of Re_{gen} studied and (b, d) presents a scaled version, in the region of the first critical point. Legend is shared. The inset in part (b) shows the rescaled version of the normalised vortex length of the tertiary eddy $(L_d - L_c)$ in the region of the second critical point.

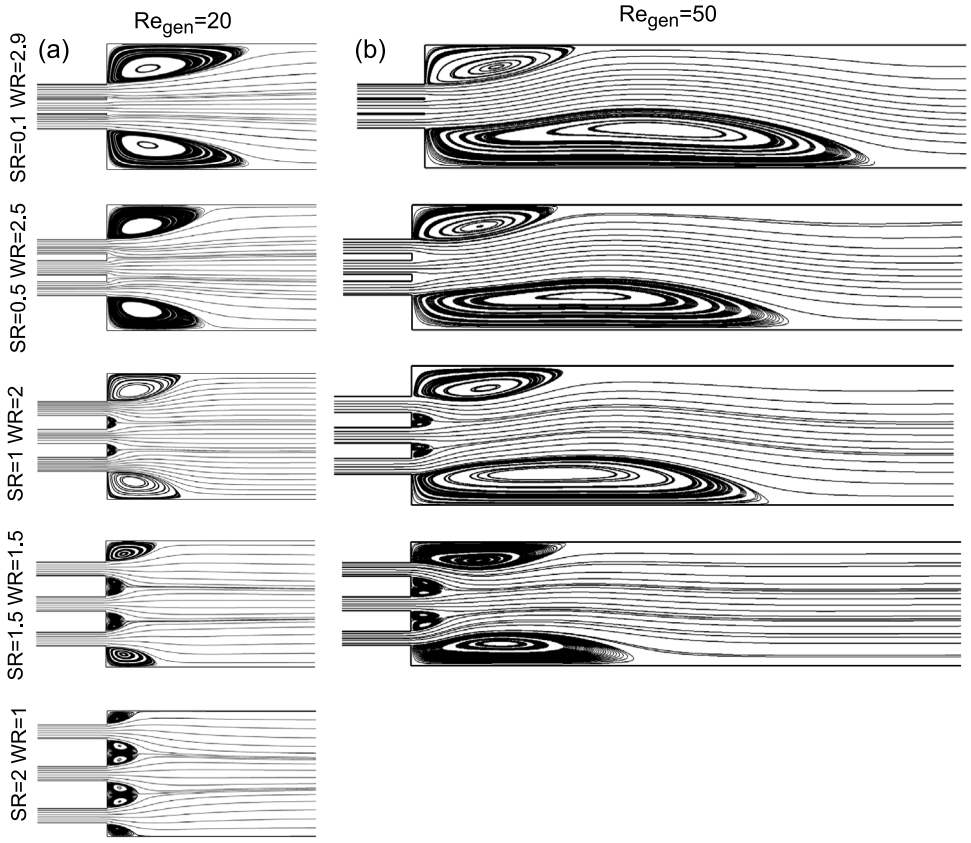

Fig. 8. Newtonian fluid flow patterns in the symmetric regime, (a) $Re_{gen} = 20$, and the asymmetric regime, (b) $Re_{gen} = 50$, for all geometries. Note that geometry E ($SR = 2$, $WR = 1$) does not exhibit a steady asymmetric regime.

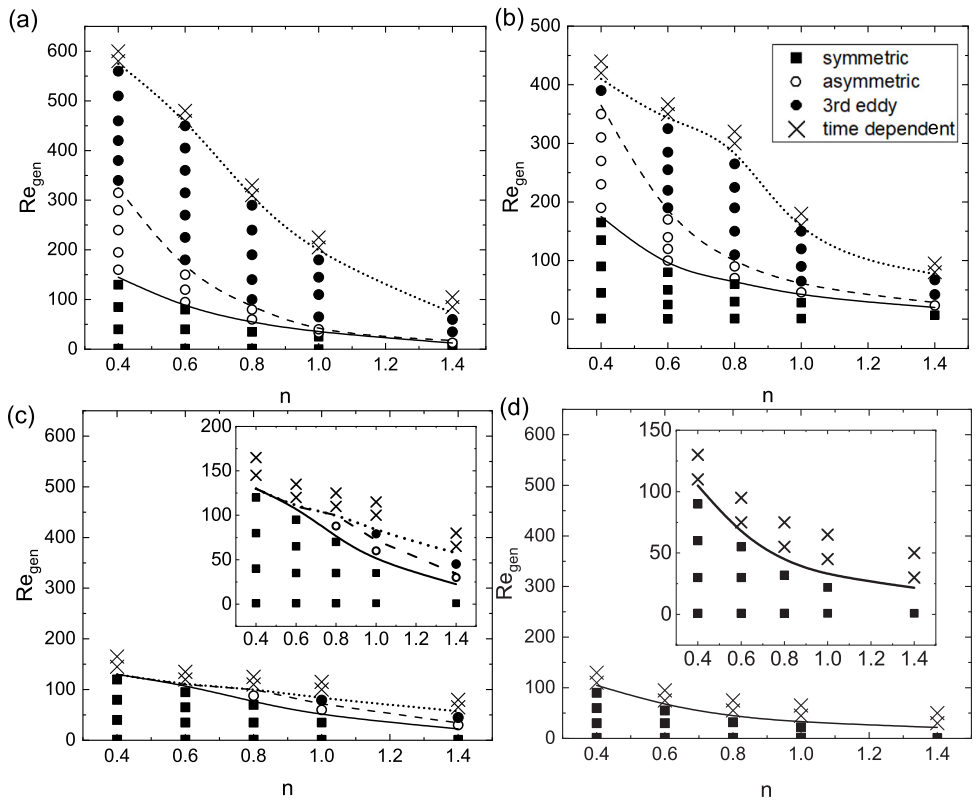

Fig. 9. Flow maps in the $Re_{gen} - n$ parameter space investigated for different geometries: (*a*) geometry A: $SR = 0.1$, $WR = 2.9$, (*b*) geometry B: $SR = 0.5$, $WR = 2.5$, (*c*) geometry D: $SR = 1.5$, $WR = 1.5$ and (*d*) geometry E: $SR = 2$, $WR = 1$. Legend is common to all plots. Lines are provided to guide the eye.

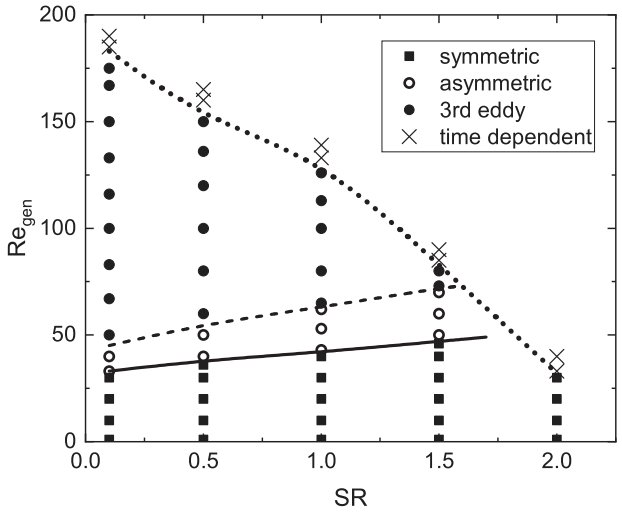

Fig. 10. Flow map in the $Re_{gen} - SR$ parameter space investigated for a Newtonian fluid. Lines are provided to guide the eye.

ER_{mod} definition instead. The larger difference between $Re_{gen,cr1}$ and $Re_{gen,cr2}$ for shear-thinning fluids when compared to shear-thickening fluids is maintained whilst varying SR, with this effect amplified at low SR and suppressed at high SR.

To better display some of the effects of changing SR, in particular the variation in the critical values of Re_{gen} as SR is increased, Fig. 10 displays the flow map in the $Re_{gen} - SR$ domain, highlighting the flow regimes present for each geometry for the Newtonian fluid.

4.3.2. The effect of WR

An interesting observation about geometry E ($SR = 2$, $WR = 1$), is its similarity to that of a single inlet expansion with $ER = 3$, the flow through which we have also simulated for comparison. Geometrically, the former can be thought of as three side-by-side expansions (each with $ER = 3$) as shown in Fig. 11. In particular, Fig. 11 illustrates the remarkable similarity between the corner vortex size and shape observed for the single inlet ($ER = 3$, $WR = 1$) and the multi inlet ($ER = 9$, $SR = 2$, $WR = 1$) configurations at two Re_{gen} within the symmetric regime. It is noted that, similarly to the corner vortex behaviour, for the multi inlet geometry the intermediate vortex pairs also grow with Re_{gen} within the symmetric regime.

Two additional single inlet expansion geometries were created, with an $ER = 5$ ($WR = 2$) and an $ER = 6.8$ ($WR = 2.9$), which exhibit the same WR as geometries C ($WR = 2$, $SR = 1$) and A ($WR = 2.9$, $SR = 0.1$), respectively. The quantitative comparison of the length of the vortices formed at the walls in the multiple inlet case and those formed in the corresponding single inlet case is shown in Fig. 12. It can be seen that although the transition to asymmetric flow is delayed to higher Re_{gen} when there are multiple inlets, the size of the corner vortices in both single and multiple inlet cases are very similar in the symmetric regime. It is also interesting to note that, between the $Re_{gen,cr1}$ for the single inlet and the $Re_{gen,cr1}$ for the multiple inlet case, the size of the symmetric vortices observed in the multiple inlet case ($L_a = L_b$) follows that of the largest corner vortex in the asymmetric regime in the single inlet case ($L_{a,single}$). The agreement is particularly good for $WR = 1$ and $WR = 2$, while for $WR = 2.9$ the differences between the single and multiple inlet cases are more noticeable. These results show that WR is a critical geometric parameter in controlling the vortex lengths in the multi inlet geometries provided the inlets are sufficiently spaced. In single inlet geometries, WR is directly related to ER ($ER = 1+2WR$), which is typically reported as the key geometrical parameter. In the multi inlet case, however ER_{mod} can be changed without varying WR, (by varying S and H, simultaneously), and so it is important to identify the effect of WR.

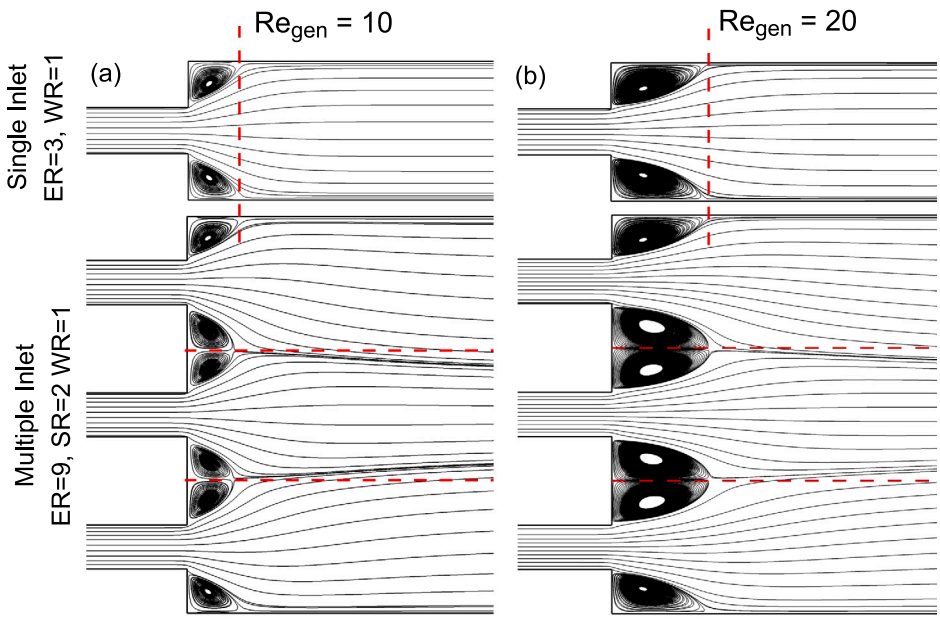

Fig. 11. Comparison of the corner vortex size between the single inlet ($ER = 3$, $WR = 1$) and multi inlet geometry E ($SR = 2$, $WR = 1$, $ER = 9$) for $n = 1$ at (*a*) $Re_{gen} = 10$ and (*b*) $Re_{gen} = 20$. The horizontal dashed lines demarcate three regions similar in geometry to that of the single inlet and the vertical lines highlight the similarity in corner vortex length.

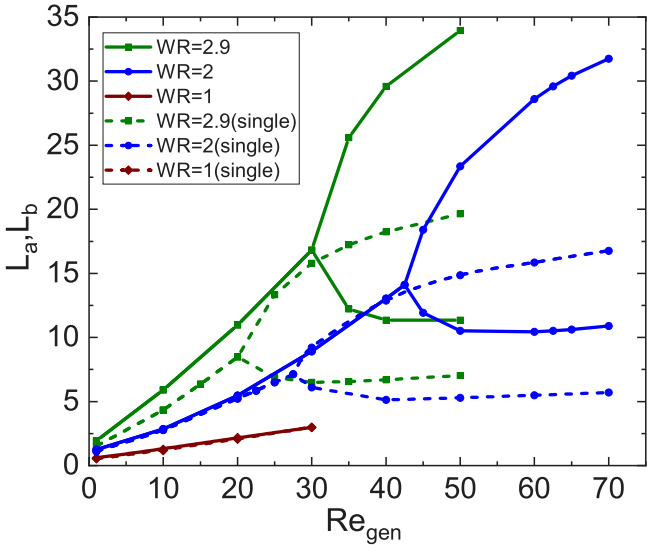

Fig. 12. Vortex length against generalised Reynolds in single and multi inlet geometries of the same WR and $n = 1$. Lines are provided to guide the eye.

5. Conclusion

We have investigated the flow through multiple inlet sudden expansions with three inlets, considering a range of inlet spacing ratios, using Newtonian, and inelastic shear-thinning and shear-thickening fluids. In doing so a number of similarities and differences were identified when compared to single inlet counterparts. Similarly to single inlet geometries, the flow exhibits symmetric vortices on the walls at low Re_{gen}, before undergoing bifurcations to the asymmetric and 3rd eddy regimes. New scalings are introduced that help collapse the data (size and intensity of the vortices) for different power-law indices.

Shear-thinning behaviour is seen to stabilise these transitions, delaying the transitions to higher Re_{gen}, whilst shear-thickening behaviour is seen to have a destabilising effect. However, in the multi inlet case, two pairs of intermediate vortices form between the streams on the walls immediately downstream of the expansion. These pairs are symmetric until $Re_{gen,cr1}$ and grow in length with increasing Re_{gen}. The flow eventually becomes time dependent as Re_{gen} is increased with this transition being strongly dependent on spacing ratio and power-law index. This gives rise to a number of different flow transitions over the range of SR, n and Re_{gen} parameter space investigated, with the flow transitioning to time dependent from different flow regimes depending on the geometrical characteristics and the fluid's power-law index. The spacing ratio is also shown to have a strong effect on the flow transitions, in particular to time-dependent flow.

The wall ratio WR is a critical geometric parameter in controlling the length of the corner vortices at high values of SR. When the spacing ratio is low and the inlet streams start to interact, SR must be considered as well. When the interaction between inlet streams is not significant, the lengths of the corner vortices are seen to be similar to those of single inlets with equivalent WR.

Declaration of competing interest

The authors declare that they have no known competing financial interests or personal relationships that could have appeared to influence the work reported in this paper.

Data availability

Data that support the findings of this study are available at https://doi.org/10.15129/469a40a7-77ff-42b7-86ae-75797e09b934.

Acknowledgements

We would like to thank Manuel Alves for insightful discussions. JC, MSNO and KZ wish to acknowledge EPSRC PhD Studentship, United Kingdom EP/W524670/1. Results were obtained using the ARCHIE-WeSt High Performance Computer (www.archie-west.ac.uk) based at the University of Strathclyde.

References

[1] C.A. Browne, A. Shih, S.S. Datta, Pore-scale flow characterization of polymer solutions in microfluidic porous media, Small 16 (2020) 1903944.

[2] L.H. Back, E.J. Roschke, Shear-layer flow regimes and wave instabilities and reattachment lengths downstream of an abrupt circular channel expansion, J. Appl. Mech. 39 (1972) 677–681.

[3] M. Vanierschot, E. Van den Bulck, The influence of swirl on the reattachment length in an abrupt axisymmetric expansion, Int. J. Heat Fluid Flow 29 (2007) 75–82.

[4] F.T. Pinho, P.J. Oliveira, J.P. Miranda, Pressure losses in the laminar flow of shear-thinning power-law fluids across a sudden axisymmetric expansion, Int. J. Heat Fluid Flow 24 (2003) 747–761.

[5] E. Lukács, J. Vad, A passive loss reduction method of square-to-square sudden expansions, Energy Build. 266 (2022) 112113.

[6] Y. Kim, H. Park, Upward bubbly flows in a square pipe with a sudden expansion: Bubble dispersion and reattachment length, Int. J. Multiph. Flow. 118 (2019) 254–269.

[7] F. Durst, A. Melling, J.H. Whitelaw, Low Reynolds number flow over a plane symmetric sudden expansion, J. Fluid Mech. 64 (1974) 111–128.

[8] R.M. Fearn, T. Mullin, K.A. Cliffe, Low Reynolds number flow over a plane symmetric sudden expansion, J. Fluid Mech. 211 (1990) 595–608.

[9] D. Drikakis, Bifurcation phenomena in incompressible sudden expansion flows, Phys. Fluids 9 (1997) 76–87.

[10] P. Ternik, J. Marn, Z. Zunic, Non-Newtonian fluid flow through a planar symmetric expansion:Shear-thickening fluids, J. Non-Newton. Fluid Mech. 135 (2006) 136–148.

[11] P. Neofytou, Transition to asymmetry of generalised Newtonian fluidflows through a symmetric sudden expansion, J. Non-Newton. Fluid Mech. 133 (2006) 133–140.

[12] S. Dhinakaran, M. Oliveira, F. Pinho, M. Alves, Steady flow of power-law fluids in a 1:3 planar sudden expansion, J. Non-Newton. Fluid Mech. 198 (2013) 45–58.

[13] W. Cherdron, F. Durst, J.H. Whitelaw, Asymmetric flows and instabilities in symmetric ducts with sudden expansions, J. Fluid Mech. 84 (1978) 13–31.

[14] N. Alleborn, K. Nandakumar, H. Raszillier, F. Durst, Further contributions on the two-dimensional flow in a sudden expansion, J. Fluid Mech. 330 (1997) 169–188.

[15] R.P. Chhabra, J.F. Richardson, Non-Newtonian Flow and Applied Rheology, second ed., Butterworth-Heinemann, Oxford, 2008.

[16] W. Ostwald, De Waele-Ostwald equation, Kolloid-Z. 47 (1929) 176–187.

[17] A.B. Metzner, J.C. Reed, Flow of non-Newtonian fluids-correlation of the laminar, transition, and turbulent-flow regions, AIChE J. 1 (1955) 434–440.

[18] R. Manica, A.L. De Bortoli, Simulation of sudden expansion flows for power-law fluids, J. Non-Newton. Fluid Mech. 121 (2004) 35–40.

[19] P. Ternik, Planar sudden symmetric expansion flows and bifurcation phenomena of purely viscous shear-thinning fluids, J. Non-Newton. Fluid Mech. 157 (2009) 15–25.

[20] P. Ternik, New contributions on laminar flow of inelastic non-Newtonian fluid in the two-dimensional symmetric expansion: Creeping and slowly moving flow conditions, J. Non-Newton. Fluid Mech. 165 (2010) 1400–1411.

[21] P. Townsend, K. Walters, Expansion flows on non-newtonian liquids, Chem. Eng. Sci. 49 (1994) 748–763.

[22] P.J. Oliveira, Asymmetric flows of viscoelastic fluids in symmetric planar expansion geometries, J. Non-Newton. Fluid Mech. 114 (2003) 33–63.

[23] M.F. Naccache, R.S. Barbosa, Creeping flow of viscoplastic materials through a planar expansion followed by a contraction, Mech. Res. Commun. 34 (2007) 423–431.

[24] R.J. Poole, M.A. Alves, P.J. Oliveira, F.T. Pinho, Plane sudden expansion flows of viscoelastic liquids, J. Non-Newton. Fluid Mech. 146 (2007) 79–91.

[25] R.J. Poole, F. Pinho, M.A. alves, P.J. Oliveira, The effect of expansion ratio for creeping expansion flows of UCM fluids, J. Non-Newton. Fluid Mech. 163 (2009) 35–44.

[26] P.C. Sousa, P.M. Coelho, M.S.N. Oliveira, M.A. Alves, Laminar flow in three-dimensional square–square expansions, J. Non-Newton. Fluid Mech. 166 (2011) 1033–1048.

[27] L.L. Ferras, A.M. Afonso, M.A. Alves, J.M. Nobrega, F.T. Pinho, Newtonian and viscoelastic fluid flows through an abrupt 1: 4 expansion with slip boundary conditions, Phys. Fluids 32 (2020) 043103.

[28] J.P. Rothstein, G.H. McKinley, Extensional flow of a polystyrene Boger fluid through a 4: 1: 4 axisymmetric contraction/expansion, J. Non-Newton. Fluid Mech. 86 (1999) 61–88.

[29] L.E. Rodd, T.P. Scott, D.V. Boger, J.J. Cooper-White, G.H. McKinley, The inertio-elastic planar entry flow of low-viscosity elastic fluids in micro-fabricated geometries, J. Non-Newton. Fluid Mech. 129 (2005) 1–22.

[30] G.H. McKinely, L.E. Rodd, M.S.N. Oliveira, J.J. Cooper-White, Extensional flows of polymer solutions in microfluidic converging/diverging geometries, J. Cent. South Univ. Technol. 14 (2007) 6–9.

[31] M.S.N. Oliveira, L.E. Rodd, G.H. McKinley, M.A. Alves, Simulations of extensional flow in microrheometric devices, Microfluid. Nanofluid. 5 (2008) 809–826.

[32] L.E. Rodd, D. Lee, K.H. Ahn, J.J. Cooper-White, The importance of downstream events in microfluidic viscoelastic entry flows: Consequences of increasing the constriction length, J. Non-Newton. Fluid Mech. 165 (2010) 61–88.

[33] R. Hidema, T. Oka, Y. Komoda, H. Suzuki, Effects of flexibility and entanglement of sodium hyaluronate in solutions on the entry flow in micro abrupt contraction-expansion channels, Phys. Fluids 31 (2019) 072005.

[34] P.P. Jagdale, D. Li, X. Shao, J.B. Bostwick, X. Xuan, Fluid rheological effects on the flow of polymer solutions in a contraction–expansion microchannel, Micromachines 11 (2020) 278–294.

[35] D. Li, L. Song, C. Zhang, L. Yu, X. Xuan, A depth-averaged model for Newtonian fluid flows in shallow microchannels, Phys. Fluids 33 (2021) 012002.

[36] H. Ameur, Pressure drop and vortex size of power law fluids flow in branching channels with sudden expansion, J. Appl. Fluid Mech. 11 (2018) 1739–1749.

[37] S. Drost, J. Westerweel, Interaction effects in multi-outlet viscoelastic contraction flow, J. Non-Newton. Fluid Mech. 213 (2014) 31–38.

[38] P.J. Oliveira, F.T. Pinho, G.A. Pinto, Numerical simulation of non-linear elastic flows with a general collocated finite-volume method, J. Non-Newton. Fluid Mech. 79 (1998) 1–43.

[39] M.A. Alves, P.J. Oliveira, F.T. Pinho, A convergent and universally bounded interpolation scheme for the treatment of advection, Internat. J. Numer. Methods Fluids 41 (2003) 47–75.

[40] A.R. Giaquinta, T.-K. Hung, Slow non-Newtonian flow in a zone of separation, J. Eng. Mech. Div. - Proc. Am. Soc. Civ. Eng. EM6 (1968) 1521–1538.

[41] S. Mishra, K. Jayaraman, Asymmetric flows in planar symmetric channels with large expansion ratio, Internat. J. Numer. Methods Fluids 38 (2002) 945–962.